

# We are IntechOpen, the world's leading publisher of Open Access books Built by scientists, for scientists

6,900

Open access books available

186,000

International authors and editors

200M

Downloads

Our authors are among the

154

Countries delivered to

TOP 1%

most cited scientists

12.2%

Contributors from top 500 universities



WEB OF SCIENCE™

Selection of our books indexed in the Book Citation Index  
in Web of Science™ Core Collection (BKCI)

Interested in publishing with us?  
Contact [book.department@intechopen.com](mailto:book.department@intechopen.com)

Numbers displayed above are based on latest data collected.  
For more information visit [www.intechopen.com](http://www.intechopen.com)



---

# Computer-Aided Physical Simulation of the Soft-Reduction and Rolling Process

---

Marcin Hojny

Additional information is available at the end of the chapter

<http://dx.doi.org/10.5772/intechopen.68606>

---

## Abstract

The chapter presents experimental problems related to research aiming at obtaining data necessary to formulate a physical model of deformation of steel containing a zone consisting of a mixture of the solid and the liquid phases. This issue is strictly related to the application of the soft-reduction process in integrated strip casting and rolling. The original part of the developed methodology is the experiment computer aid performed with the proprietary simulation package DEFFEM. In order to solve problems related to the deformation of materials with a semi-solid core or at extra-high temperatures, comprehensive tests were applied, which covered both physical modelling with a Gleeble 3800 thermo-mechanical simulator and mathematical modelling. Examples of research findings presented in this chapter show that the developed methodology is correct in the context of experiment computer aid and show the need to develop software in order to implement full 3D models.

**Keywords:** mushy zone, finite elements method, extra-high temperature, resistance heating, tomography

---

## 1. Introduction

In recent years, a strong trend towards the development of integrated metallurgical processes can be observed. In these processes, the strand is cast to shape and dimensions near the final product and combined with product rolling [1–7]. Processes of integrated strip casting and rolling, which feature less material processing, and a direct connection of the casting process and strand rolling, can be used as an example. Here, problems related to the steel ductility and the formation of an appropriate product microstructure are very relevant. During an integrated process, contrary to classic hot forming processes, the strand is not cooled to a temperature at which austenite disintegrates [1–7]. Therefore, the original structure of the input

---

material to the rolling process is the as-cast structure, which causes serious difficulties during the production cycle. The increasing access to modern Gleeble series physical simulators allows us to use the knowledge obtained during experiment with tests of designing processes of strip integrated casting and rolling [8, 9]. A Gleeble 3800 simulator enables the so-called physical simulation of a specific process to be carried out. The objective of a simulation like this is to use a small sample, which is made of the same material that is used in the production process. Changes of stress, strains and temperatures, the material is subjected to in the actual production process, are reconstructed in the mentioned sample, which most often is cylindrical [10]. On the basis of the performed physical simulation cycle (variants for various cooling rates, stroke rates, etc.), process maps are developed, and then these maps help to estimate the optimal parameters of the process line equipment. Special diagrams are then constructed, where areas with a limited ductility are marked. Knowing such areas thoroughly allows the process parameters to be adjusted so as to avoid potential strand cracking. Despite huge capabilities of thermo-mechanical simulators as regards a simulation combining a physical simulation of solidification with a simultaneous plastic deformation set during, as well as immediately after the total solidification, each steel grade requires separate comprehensive tests. Therefore, a computer simulation is recommended. The main problem with computer simulations involves lack of constitutive equations, which allow the plastic behaviour of the steel tested to be determined. We need to emphasize that testing mechanical and physical properties, as well as the sample deformation itself at such high temperatures is only possible to a limited extent, with a strictly specified test methodology [10]. Therefore, the goal of this study is to develop a methodology to enable a multi-stage simulation combining the steel deformation process in the semi-solid state and in the solid state, as well as to evaluate its suitability for the future research and development work.

## 2. Physical simulation

The experimental tests were conducted with a Gleeble 3800 thermo-mechanical simulator. The basic tests were conducted with cylindrical samples made of steel S355, with a length of 125 mm and a diameter of 10mm, using two types of copper grips, so-called “hot” and “cold” ones. The selection of an appropriate grip type determines the attainable size of the free zone of the sample deformed [10]. For “cold” grips, the free zone is about 30mm, whereas for “hot” grips, it is about 67mm. In addition, the type of the applied grips substantially influences the attainable width of the remelting zone, which increases as the nominal test temperature increases, and the obtained temperature gradient along the heating zone and on the sample cross-section [10]. During the tests, the temperature was recorded as indicated by thermocouples: TC1 (near the place of the sample-grip contact), TC2 (at a distance of 7.5mm from the heating zone centre), TC4 (the centre of the heating zone, control thermocouple) and TC3 (temperature measurement within the sample core) (**Figure 1**).

Changes in force versus tool movement, and changes in electrical current versus time were additional values measured during the experiments. From the perspective of methodology development one should take into account the temperatures that are characteristic to the

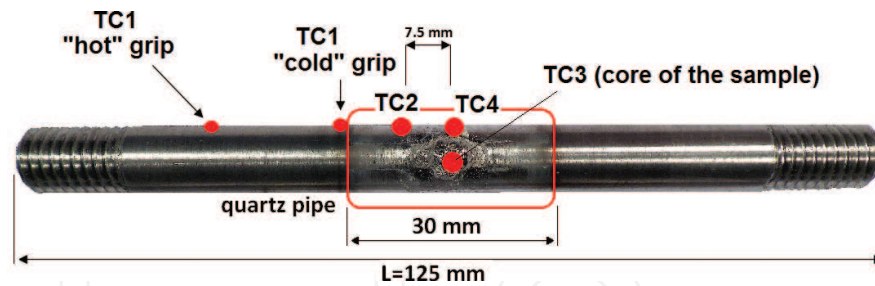


**Figure 1.** A cylindrical sample used during experiments with the thermocouple location.

specific tested material [10]. The liquidus  $T_l$  and solidus  $T_s$  temperatures, the nil strength temperature (NST), the nil ductility temperature (NDT) and the ductility recovery temperature (DRT) are the most important. The determined characteristic temperatures allow a thermal map of the process (TMP) to be developed. This map allows us, among others, to determine the temperature ranges in which the liquid phase appears or disappears, or the temperature above which the mechanical properties of the medium analysed degrade. For steel S355 the liquidus  $T_l$  and solidus  $T_s$  temperatures were 1513 and 1465°C, respectively. The knowledge of characteristic temperatures allows us also to determine the steel susceptibility to fracture, which is characterised by the following fracture resistance indicator  $R_f$ :

$$R_f = \frac{\text{NST} - \text{NDT}}{\text{NDT}} \quad (1)$$

Under the procedure of continuous casting physical simulation [10], it is assumed that the steel tested is not susceptible to cracking when the difference between the temperature NST and NDT is less than just 20°C. Referring to the characteristic temperatures NST and NDT of the steel S355 tested, which are 1448 and 1420°C respectively, it can be observed that this condition is not met. It indicates that the steel tested is susceptible to cracking during the production cycle. More details concerning the determination of temperature characteristics of steel S355 can be found in publications [8–10]. The execution of experiments at temperatures reaching the solidus temperature range required a strictly planned and controlled experiment course. **Figure 2** presents the view of a sample at three selected stages of physical simulation, where remelting within the liquidus and solidus temperature range was performed. At the first stage (left) one may observe the explicit remelting zone (a mixture of the solid and liquid phases) being formed. At the second and third stages (middle and right), when the deformation started, an adverse effect of liquid steel blow-out occurred within the remelting phase. In order to eliminate this problem the orientation of the injection nozzles situated perpendicularly to the sample was changed to an



**Figure 2.** The view of the sample at the selected physical simulation stages (S355 grade steel).

angle of about  $45^\circ$ . This change stabilized the injection, by reducing the blowing of the liquid steel out of the sample.

The problem of an uncontrolled leakage was also observed for deformation within the mixed phase using relatively low tool stroke rates between 1 and 20 mm/s. Using a tool stroke rate of around 100 mm/s allowed us to fully accomplish the assumed experiment plan [10]. Therefore, one may conclude that the obtained pilot simulation results open and indicate new research areas directed towards high stroke rate testing. In a part of the primary tests, in order to reduce the risk of liquid steel leakage into the simulator, a quartz shield was applied with a length of about 30 mm, and a gap of 2–3 mm along the shield in order to enable thermocouples to be installed (**Figure 1**). Another problem encountered during the tests was the occurrence of rapid strength changes. One of the basic relationships determining the plastic behaviour of metal at a very high temperature is the dependence of the yield stress on temperature, strain rate and the strain. The plastic deformation at higher temperatures is subject to a number of further restrictions. The material changes its density during cooling, and at a certain temperature range it shows a limited formability or complete lack of ductility. The occurring large inhomogeneity of deformation, and the fact that even small temperature changes in these conditions cause rapid changes in the yield stress, lead to diverging results. **Figure 3** presents examples of results of maximum forces achieved during two identical compression tests at the selected nominal temperatures of deformation. On the other hand, **Figure 4** presents examples of results of maximum values of tensile stress for two identical tests at the selected nominal temperatures of deformation. The presented results concern tests conducted with steel C45 (carbon content 0.45%). For temperature measurements also slight temperature measurement differences were observed, reaching a few degrees [10]. Therefore, as mentioned before, the sample deformation itself at such high temperatures is only possible to a limited extent, with a strictly specified test methodology.

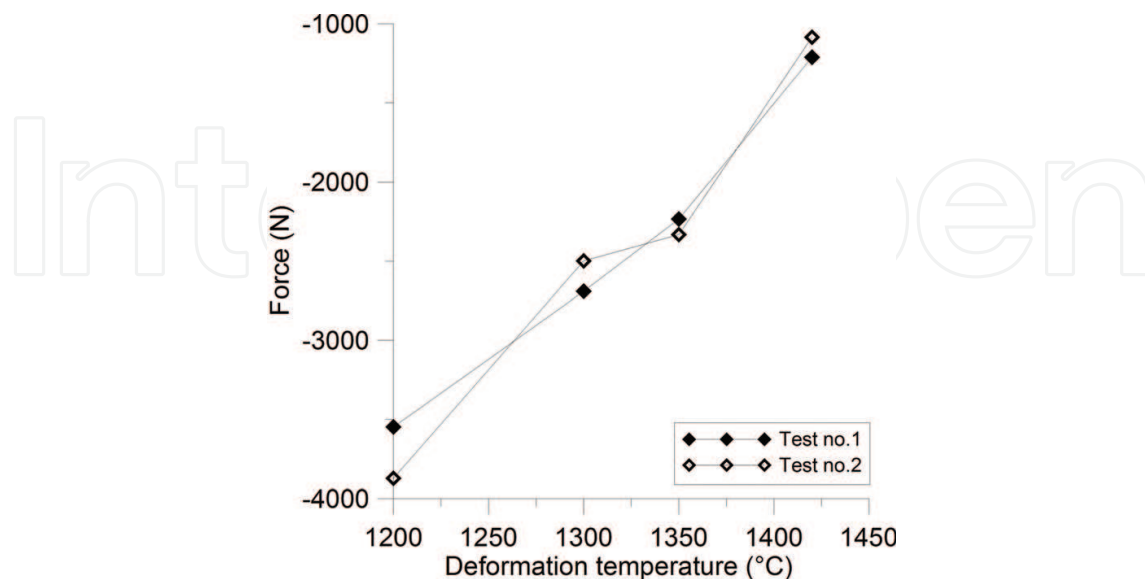


**Figure 3.** The maximum values of forces achieved during compression tests for the selected nominal temperatures of deformation.

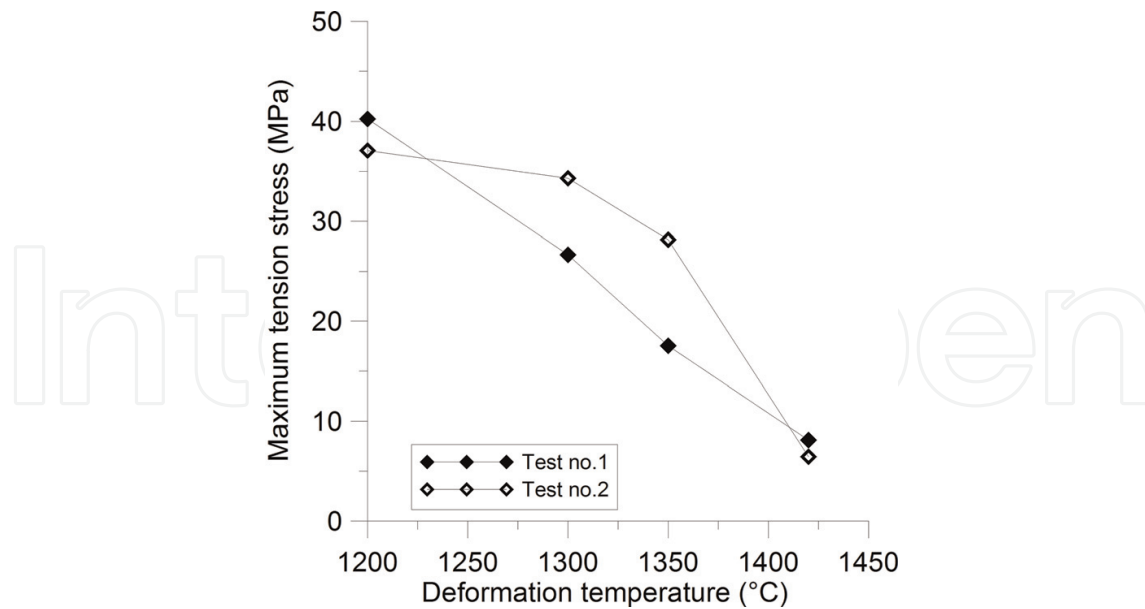


**Figure 4.** The maximum values of tensile stress achieved during tests for the selected nominal temperatures of deformation.

The adopted test methodology included:

- developing and conducting a physical simulation cycle,
- developing a numerical model of resistance heating in the Gleeble 3800 simulator system,
- developing a new methodology of direct determination of the strain-stress relationship on the basis of data obtained from physical simulations,
- test simulations with the DEFFEM package and experimental verification of the developed methodology. The tests were combined with a cycle of micro and macrostructural tests.

As part of the starting physical simulation, three experiments were carried out. The fundamental difference between these experiments was in the execution of deformation in various phases of the process. In the first test, the sample was deformed in the remelting phase. The experiment schedule consisted of heating the sample to a temperature of 1400°C at a heating rate of 20°C/s, in the next stage, the heating rate was reduced to 1°C/s until the temperature of 1485°C was reached. The third stage was holding at a temperature of 1485°C for 30s in order to stabilize the temperature within the sample volume. The last stage was the deformation in the remelting phase (stroke=1.2mm and stroke rate=0.04mm/s). The first three stages of the second test were analogous to the first test. The last stage was the execution of the deformation process (stroke=1.5mm and stroke rate=0.25mm/s) in the solidification stage, starting when the sample has cooled down. The third test was a combination of the first and the second ones. The deformation was executed in the remelting phase (stroke=1.2mm and stroke rate=0.04mm/s), and next in the solidification stage (stroke=1.5mm and stroke rate=0.25mm/s). **Figures 5–7** present macrostructures of samples for individual tests. Their nature differs depending on the applied tool variant. After the process of sample etching, the occurrence of a columnar zone was found in the

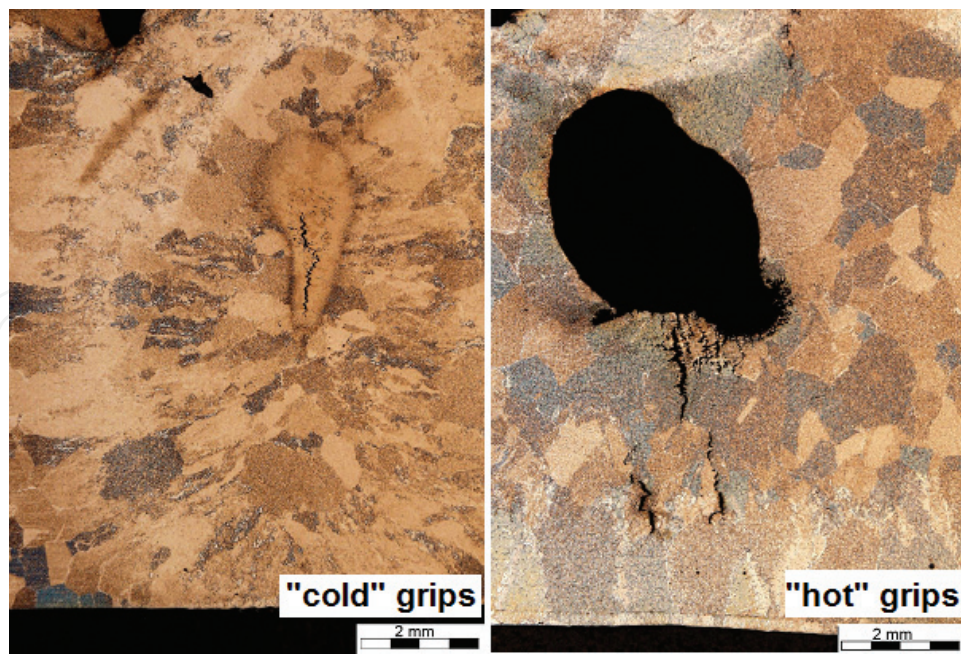


**Figure 5.** Macrostructure of samples deformed in the remelting phase (“hot” and “cold” grips).

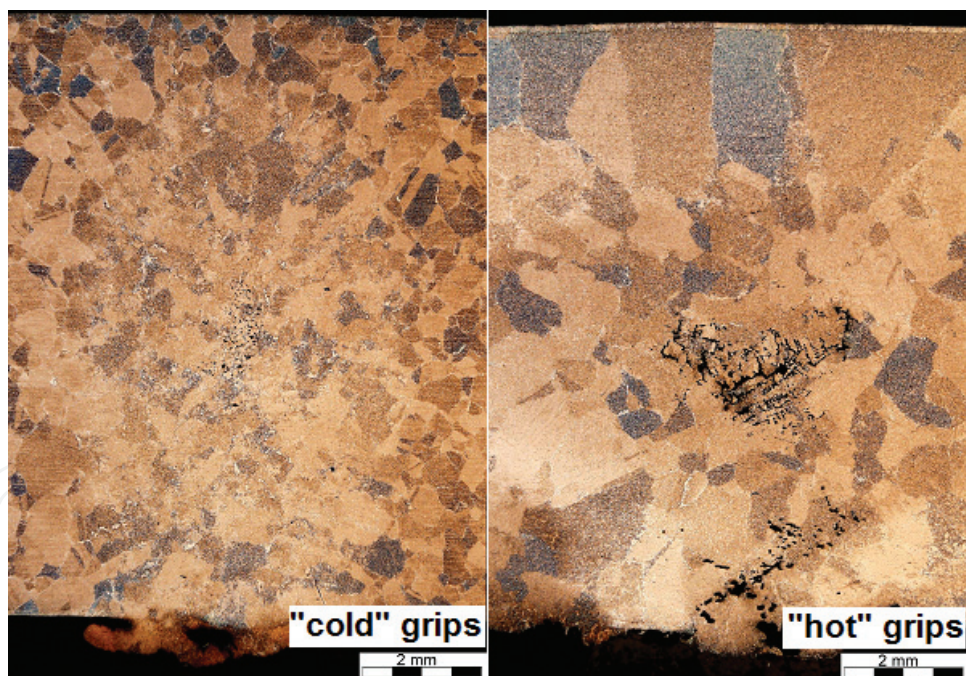


**Figure 6.** Macrostructure of samples deformed in the solidification phase (“hot” and “cold” grips).

remelting zone. The crystals were growing in the heat discharge direction (Figures 5–7). When analysing macrostructures made in the sample longitudinal section, the formation of porous areas of various intensities can be observed (Figures 5–7). Here, the variant of selected experimental tools is very important. For the variant with “hot” grips and deformation in the remelting phase (Figure 5), the formation of a large shrink hole was observed. Application of deformation

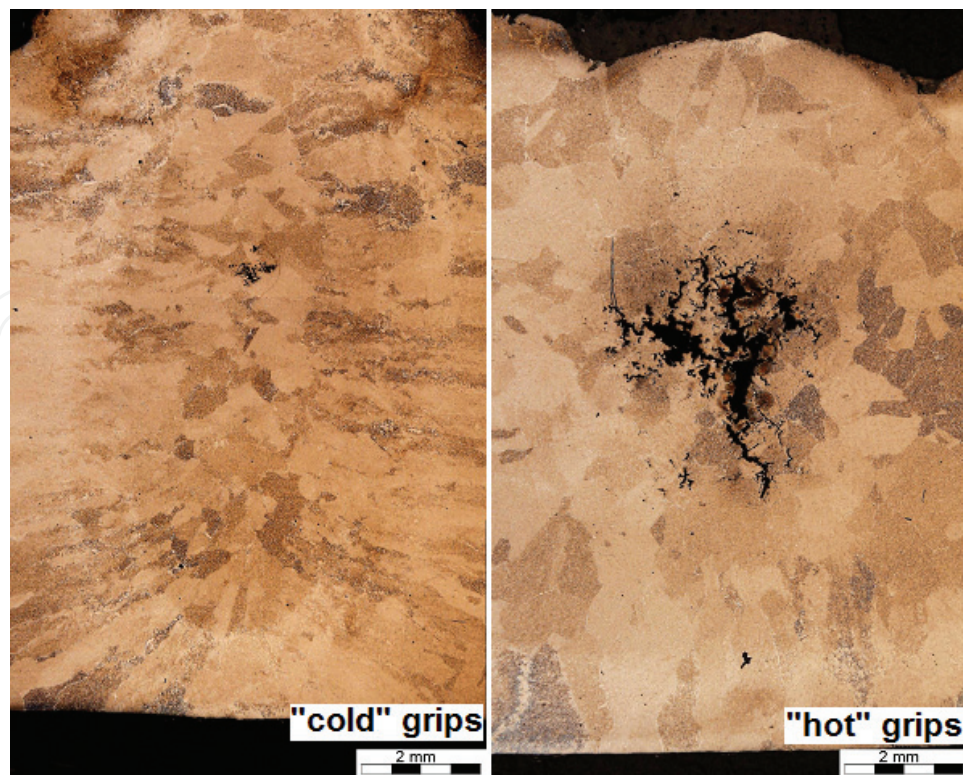


**Figure 7.** Macrostructure of samples deformed in the remelting and solidification phase (“hot” and “cold” grips).

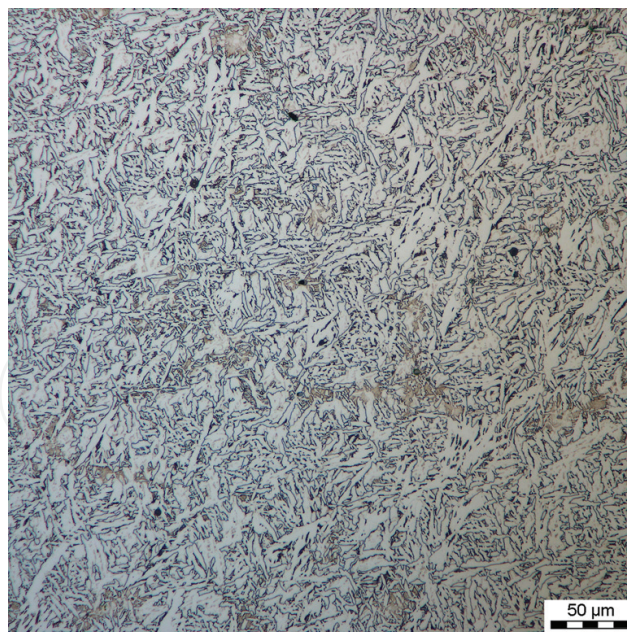


**Figure 8.** Microstructure of samples deformed in the solidification phase (core, “hot” grips).

in the solidification phase partially eliminated this effect (**Figure 6**). However, analyses of the macrostructure for the “hot” grip variant still showed small areas of central porosity (**Figures 6 and 7**). It may indicate that the applied strain value is insufficient.

**Figures 8–11** present examples of microstructures of the selected two areas of the sample, i.e. the sample core and a place located next to the sample tip (near the place of thermocouple installation) for both tool variants. Analysing the sample centre microstructure (**Figures 8 and 10**), we can detail white (slightly needle-shaped) ferrite and/or bainite. The former austenite is mainly martensite formed after cooling to the ambient temperature, and it is more dominating for the simulation variant carried out with cold grips (**Figure 10**). Martensite is light brown

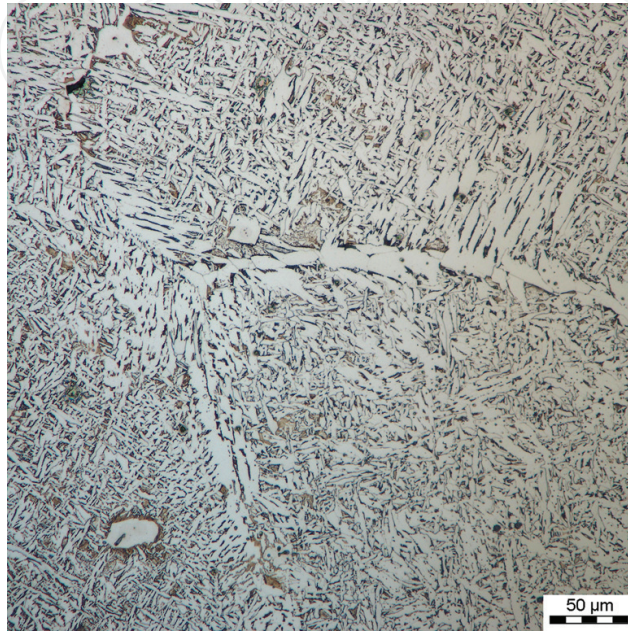


**Figure 9.** Microstructure of samples deformed in the solidification phase (tip, "hot" grips).

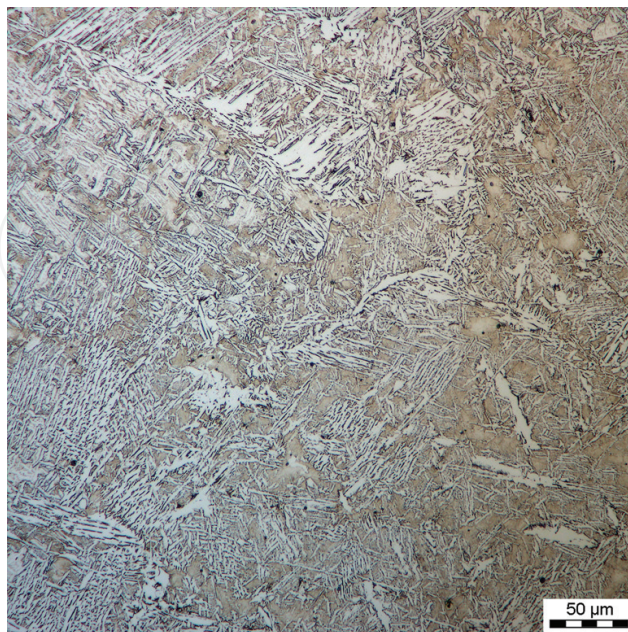


**Figure 10.** Microstructure of samples deformed in the solidification phase (core, "cold" grips).

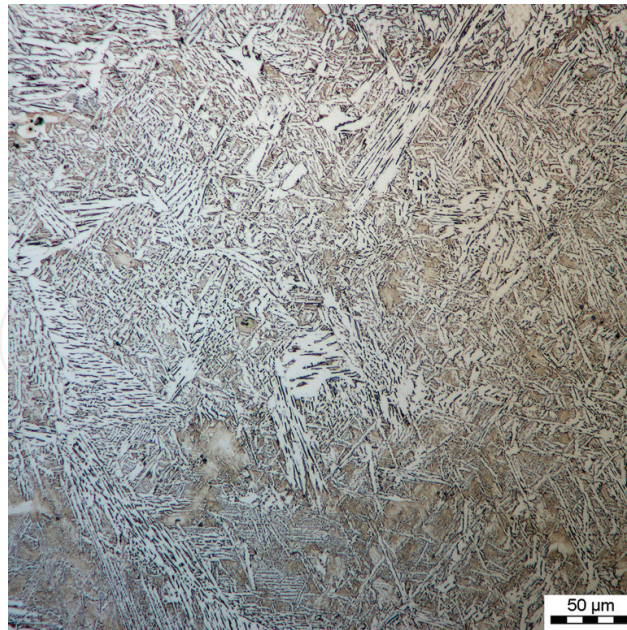


**Figure 11.** Microstructure of samples deformed in the solidification phase (tip, “cold” grips).

in the presented microstructures. The analysis of the microstructure of the surface zones (**Figures 9** and **11**) shows a slightly different nature of the share of individual phases. The obtained differences arise mainly from the cooling rate, which is two times lower for the samples heated in hot grips, and from the difference in the cooling rates between the individual zones of the sample deformed.

The conducted first cycle of physical simulations allowed us to plan and carry out a pilot simulation of the integrated strip casting and rolling process. In the performed simulation, the deformation process was conducted in crystallization phase and finally rough-rolling simulation was made. The main goal of deformation in the crystallization stage was to ensure the filling of the full volume of the remelted sample as well as to eliminate shrinkage effects. The second cycle of physical simulations included tests aiming at providing data to the computer-aided methodology of determination of the strain-stress relationship, necessary to build the model of changes in stress versus strain, strain rate and temperature for the needs of numerical simulations. The results of computer-aided physical simulations are presented hereinafter.

### 3. Computer aid of experiment

As part of the computer-aided experiment the proprietary simulation package DEFFEM [10] according to the ONEDES (ONEDEcisionSoftware) was used. More information on the simulation system designed, details of the implemented mathematical models, or definitions of boundary conditions may be found in book [10] or in the author’s second chapter in the current book.

### 3.1. Modelling the resistance heating

The process of numerical modelling a high-temperature experiment performed with a Gleeble 3800 thermo-mechanical simulator can be broken down into two main stages. At the first stage the process of sample resistance heating and melting is performed according to a set programme. This stage is very important from the perspective of the specificity of the process analysed, where even small temperature changes may locally cause rapid changes in mechanical properties. As accurate estimation of the temperature distribution within the sample volume as possible will significantly determine the quality of the obtained findings, including the determined strain-stress relationships, which ultimately will strongly influence the process force parameters of the deformation process itself (stage 2). In the first modelling approach, a commercial simulation system ANSYS was used, and the obtained final temperature field was then read in by the DEFFEM solver as the initial condition for the deformation process performed [11]. Resistance heating was modelled with an additional magnetohydrodynamical (MHD) module. This additional program extension concerns the effect of electromagnetic field and the electrically conducting medium. The module enables the conductor behaviour influenced by a constant and variable electromagnetic field to be analysed. In this study, the method in which the current density is the result of the solution of the electrical potential equation and Ohm's law was used. The electrical field is described by equation:

$$\vec{E} = -\nabla\varnothing \quad (2)$$

where  $\varnothing$  is the electric potential.

The current density is calculated from Ohm's law.

$$\vec{j} = \sigma \vec{E} \quad (3)$$

where  $\sigma$  is the specific conductance.

For a medium with a high conductivity, the principle of electric charge conservation is met additionally.

$$\nabla \cdot \vec{j} = 0 \quad (4)$$

The ANSYS program solver solves equations of continuity, moment, energy and electric potential iteratively in a loop. The energy equation contains an additional energy source, Joule's heat.

$$Q = \frac{1}{\sigma} \vec{j} \cdot \vec{j} \quad (5)$$

where  $Q$  is the Joule's heat;  $j$  is the current density vector.

A number of simulations were performed, where various heating schedules were used and their impact on the obtained final temperature field was analysed. In the model tests alternatively

both types of grips were used. It was found that the grips had a substantial impact on the attainable heating rate to the nominal deformation temperature. **Figure 12** presents the temperature changes measured by a numerical sensor placed on the sample surface (1/2 of the heating zone length). Heating simulations for both variants of tools were performed with a constant current intensity of 2000 A, assuming the heating time of 66 s. The obtained difference of the maximum calculated temperatures for both tool variants was 123°C. Regardless of the adopted temperature schedule, grip type or the grade of the steel tested, the distribution of generated voluminal sources is parabolic (**Figure 13**).

Regardless of the applied grips the temperature gradient was observed both on the cross-section and on the longitudinal section of the sample (**Figure 14**). For a sample heated with a

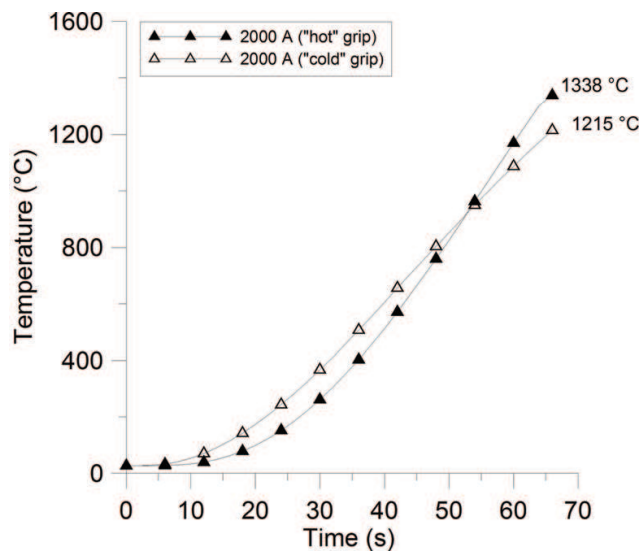


**Figure 12.** Change in the surface temperature of a sample heated with two types of grips (current intensity 2000 A).

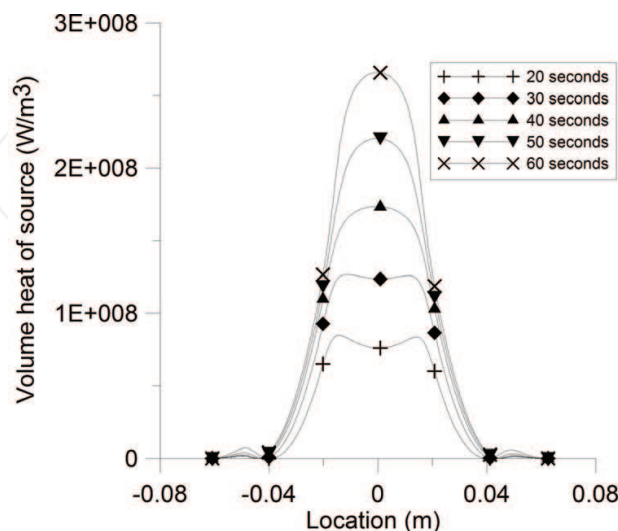


**Figure 13.** The distribution of voluminal heat sources in the sample Z axis for the selected resistance heating stages ("hot" grips).

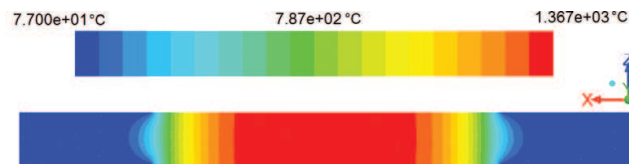


**Figure 14.** Temperature distribution on the sample section after 66s of heating (“hot” grips, current intensity 2000 A).

2000 A current for 66s using “hot” grips, the achieved sample surface temperature was 1338°C, while the core temperature was 1367°C. The temperature difference between the sample core and the surface (nominal temperature) was therefore 29°C. The current intensity characteristics is a relevant control parameter in the numerical model, which is decisive to the attainable nominal temperature of the test (possibility for remelting). For instance, a change in the current intensity from 2000 to 1000 A caused a decrease in the amount of heat generated within the system, which translated into the attainable maximum temperature of 366°C for the sample core (**Figure 15**).

In the second model approach the ADINA commercial system was used, in which the temperature field solution was based upon the classic solution of Fourier’s equation combined with inverse calculations [12, 13]. Assuming a constant current intensity, and on the basis of temperatures measured during the experiments, the values of voluminal heat sources were selected so as to obtain compatibility of results with experimental findings. Alternatively a constant value of voluminal heat sources was assumed (constant for a single simulation time interval, estimated previously with commercial simulation systems, e.g. **Figure 15**), and next the current intensity was determined. The adopted model assumptions not only allowed results featuring the correct compatibility with the experimental findings to be obtained, but also lead to an ambiguity of the solution. Examples of results using the foregoing approaches can be found in papers [12–15]. Regardless of the adopted model approach the calculations were very time consuming and painstaking. This moment has inspired the author and has resulted in the ONEDES term (ONEDEcisionSoftware) as an approach philosophy for designing dedicated original simulation systems [9, 10]. Intensive support of the Polish National Science Centre as part of research projects and huge amounts of time sacrificed by the author for the implementation of the developed solutions allowed a globally unique tool dedicated for aiding high-temperature processes to be developed. The effect of the design-implementation work was the development of a resistance heating model in the Gleeble 3800 simulator system (ONEDES approach) and the experimental verification methodology. When modelling the Joule heat generation, it was assumed that its equivalent in the numerical model would be a voluminal heat source (function  $A$ ) with its power proportional to the resistance  $R$  and the square of electric current  $I$ :

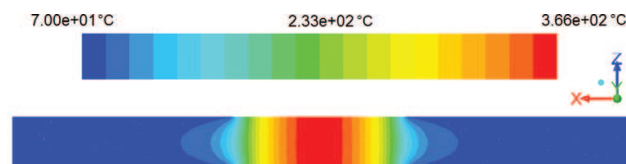


**Figure 15.** The temperature distribution on the sample section after 66s of heating (“cold” grips, current intensity 1000 A).

$$Q = f(A(\tau)[I^2(\tau)R(T)]) \quad (6)$$

The relationship of the current intensity change as a function of heating time are directly recorded during physical tests with Gleeble 3800 thermo-mechanical simulator. **Figure 16** presents examples of results in the form of temperature change versus time measured (thermocouples TC1, TC4, see **Figure 1**) and calculated (numerical sensors) during physical and computer simulations of sample heating to a temperature of 1485°C (steel S355).

The heating process was performed with two heating rates: to the temperature of 1450°C at a rate of 20°C/s, and next at a rate of 1°C/s to the nominal temperature of 1485°C. On the other hand, **Figure 17** presents temperature changes versus time measured and calculated during physical and computer simulations of sample heating to the temperature of 1200°C (steel S355) at a constant rate of 5°C/s.

The obtained graphs feature a very good compatibility between the calculated and experimentally determined temperatures. The estimated relative error oscillated within 2–3%. **Figures 18** and **19** present the temperature distribution on the longitudinal section of the sample and the symmetry with respect to the Z axis, after 3 s of heating, and after heating to the test nominal temperature of 1485°C, respectively. The simulations were conducted with “hot” grips. Analysing **Figure 18** one can observe an intensive temperature gradient near the place of tool-sample contact. The temperature gradient on the sample section at this simulation stage features a practically uniform temperature distribution of around 60°C, achieving its maximum value of 48°C after heating to a temperature of 1485°C.

The application of the simulation variant using “cold” grips leads to slightly different results (**Figure 20**). The attainable width of the remelting zone becomes shorter. In addition, one can observe that the obtained gradient on the sample section of 37°C is smaller than for the variant with “hot” grips (**Figure 19**).

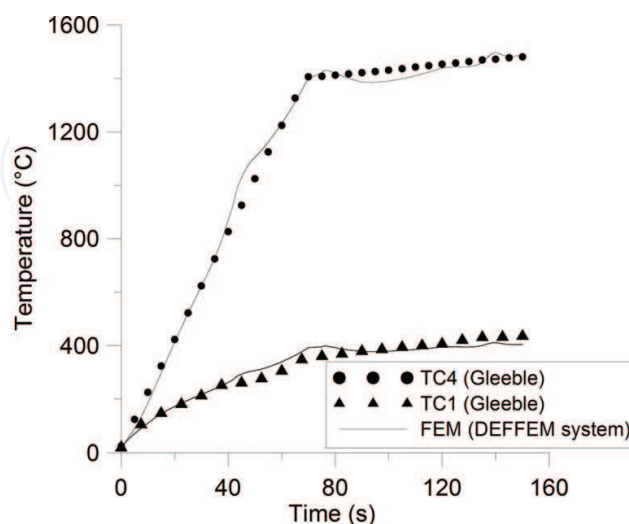


**Figure 16.** Temperature changes versus time obtained as a result of the experiment and computer simulation (thermocouples TC4 and TC1, “hot” grips).

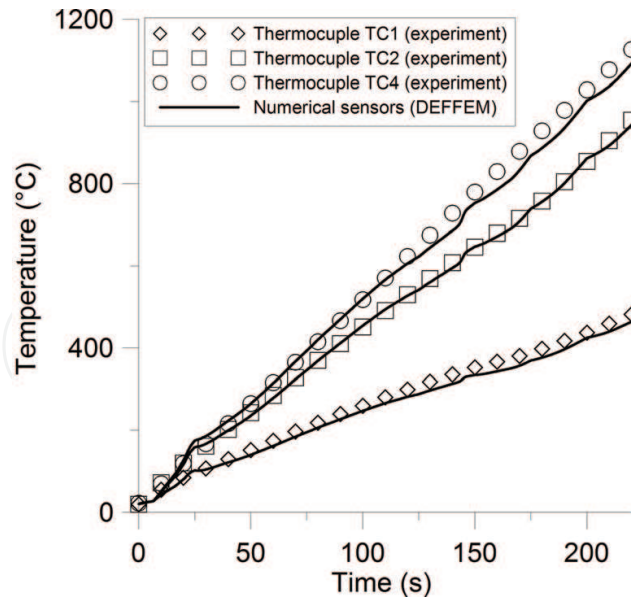


**Figure 17.** Temperature changes versus time obtained as a result of the experiment and computer simulation (thermocouples TC4, TC2 and TC1, “cold” grips, heating rate 5°C/s).

60,101	59,479	58,856	58,234	57,612	56,99	56,367
55,745	55,123	54,501	53,878	53,256	52,634	52,012
51,389	50,767	50,145	49,523	48,9	48,278	47,656
47,034	46,411	45,789	45,167	44,545	43,922	43,3
42,678	42,055	41,433	40,811			



DEFFEM |pre&post

**Figure 18.** Temperature distribution on the sample section after 3s of heating (“hot” grips).

The obtained results of computer simulations of the resistance heating process feature a considerable compatibility with the results obtained by physical simulations (for both tool variants). In the implemented numerical solution, couplings of the electrical field and the temperature field were not included directly. The heat that is generated within the sample volume as a result of the electrical current flow is modelled by an internal voluminal heat source. By applying this approach, the influence of the changing electrical properties of the solution domain (sample volume) on the electrical charge density and local voluminal heat source power could not be analysed. It is difficult to state that taking the thermo-electrical impact into account would constitute significant progress and would allow more precise results to be obtained. More details can be found in publication [10].

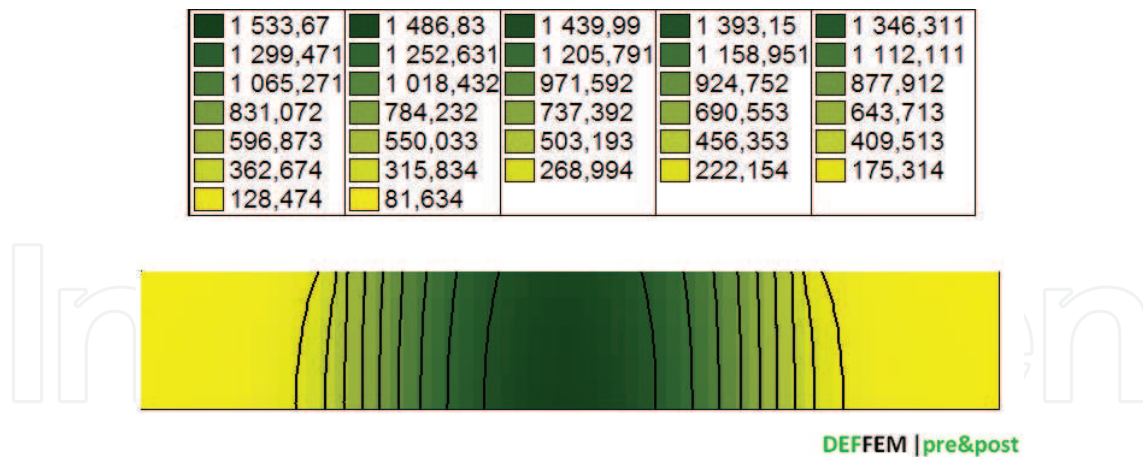


**Figure 19.** Temperature distribution on the sample section after heating to the nominal temperature of 1485°C (“hot” grips).

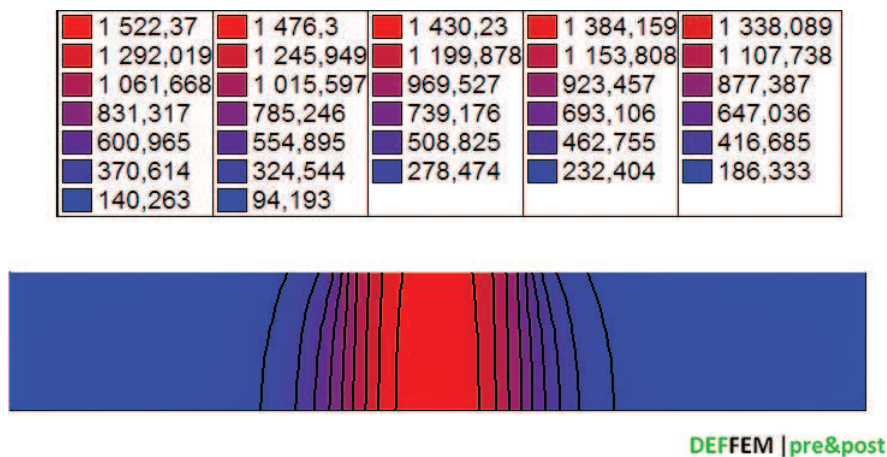


**Figure 20.** Temperature distribution on the sample section after heating to the nominal temperature of 1485°C (“cold” grips).

### 3.2. The methodology of direct determination of mechanical properties (S355 grade steel)

The problem of determining characteristics describing changes in stress versus strain, strain rate and temperature is a very complex issue. As showed by research presented herein, the repeatability of test as regards anticipating changes in temperature or force parameters may significantly differ between two identical tests (see **Figures 3** and **4**). In the context of determining mechanical properties, the accuracy of determination of the temperature field becomes therefore particularly significant. It is caused by the fact that even small local temperature variations may cause rapid changes in mechanical properties. One of methods applied by the author was the use of a methodology [Numerical Identification Methodology (NIM)] based upon the inverse solution and a methodology of modelling with a model concept based upon axially symmetrical models [10]. As part of the current project (3D model development), it has been found that this approach is ineffective in terms of computing, as well as of the quality of

the obtained curves. Depending on the adopted solution of the model resistance heating process in the aspect of the temperature field determination (inverse calculations, temperature field from the commercial program, or the function description presented herein), it leads to slightly different temperature values within the deformation zone. Bearing in mind that mechanical properties rapidly change as a result of small temperature fluctuations, the obtained stress-strain curves are considerably different (their nature). In the context of verification of the yield stress function model, the obtained results of the process force parameters or the deformation zone shape itself showed a convergence with the experimental data. Thus a question comes: which approach in the context of modelling of mechanical properties at such high temperatures is the optimum solution? It was one of the factors that inspired the author to take up implementing and development work in the context of formulating a full multi-scale 3D model of high-temperature effects. Therefore, as part of project work, the Direct Identification Methodology (DIM) to determine the mentioned dependences directly was developed. The DIM utilizes the capabilities of the Gleeble 3800 simulator as regards experimental research, and the original DEFFEM simulation system for identification of model parameters [10]. The proposed research methodology consists of the following stages: In the first stage samples are prepared for tests, along with the installation of measurement thermocouples, and copper grips and the experiment programme are selected [10]. The second stage includes physical tensile tests on the basis of the assumed physical simulation schedule. The experiment programme included heating to a temperature of 1400°C at a rate of 20°C/s, and next to a temperature of 1480°C at a rate of 1°C/s. Finally, cooling to the nominal deformation temperature was made at a rate of 10°C/s, and after holding for 10s at the set temperature the deformation process (tension test) was made with stroke 0.5–2mm and a tool stroke rate of 1 and 20mm/s. In the third stage, the preliminary simulations in order to estimate the length of the deformable zone are performed. On the basis of the preliminary test results, as well as the analysis of the temperature fields, the length  $L_0$  of the effective working zone can be estimated at 20mm. Within this zone, the strain rate and the stress are supposed as uniaxial. The nominal strain  $\varepsilon_{nom}$  and the nominal strain rate  $\dot{\varepsilon}_{nom}$  are defined as follows:

$$\varepsilon_{nom} = \frac{\Delta L}{L_0} \quad (7)$$

where  $\Delta L$  is the grip stroke (the elongation of the effective working zone at time  $\tau$ ) and  $L_0$  effective working zone.

$$\dot{\varepsilon}_{nom} = \frac{stroke\_rate}{L_0} \quad (8)$$

The nominal stress is calculated with the following relationship:

$$\sigma_{nom}^{exp} = \frac{F}{S_0} \quad (9)$$

where  $F$  is the tensile force measured by the Gleeble 3800 simulator and  $S_0$  is the original cross-sectional area of the sample. In the fourth stage, the yield stress function form is selected. In the

presented solution, the function form describing the dependence of the nominal stress on the nominal strain is the function in the following form [10]:

$$\sigma_{nom}^{exp} = \frac{\varepsilon_{nom}^n}{\alpha} \text{ASINH} \left[ \left( \frac{\dot{\varepsilon}_{nom}}{A} \right)^m \exp \left( \frac{mQ}{RT_{nom}} \right) \right] \quad (10)$$

The last parameter that should be defined in function (10) is the value of the nominal temperature  $T_{nom}$ . In this study, the nominal temperature was defined as the sample surface temperature:

$$T_{nom} = T_{surf}^{exp} \quad (11)$$

In the last stage of the proposed methodology, the objective function for the purpose of identification of the searched parameter vector  $x = (\alpha, n, A, m, Q)$  of the function (10) is defined [16]:

$$\varphi(x) = \frac{1}{N_t} \frac{1}{N_{pr}} \sum_{i=1}^{N_t} \sum_{j=1}^{N_{pr}} \left[ \frac{\sigma_{nom,ij}^{calc}(x) - \sigma_{nom,ij}^{exp}}{\sigma_{nom,ij}^{exp}} \right]^2 \quad (12)$$

where  $N_t, N_{pr}$  are the number of tensile tests and measurement points, respectively.  $\sigma_{nom}^{calc}, \sigma_{nom}^{exp}$  are the nominal stress from calculations and experiments, respectively.

The searched parameter vector  $x$  can be identified by minimization of the objective function (12). Gradient-free optimisation was used to minimize the objective function (12). The identified parameters of vector  $x$ , based on the DIM, are presented in **Table 1**.

The calculated and deduced nominal stress-strain curves are shown in **Figures 21–26**. All measurement points obtained from the experiment are included in the graphs, in order to present the scatter of the experimental data. Before using them in the optimisation procedures, such data were previously subjected to a smoothing procedure. A reasonable agreement can be observed between the calculated and the directly predicted nominal stress-strain curves. The mean relative errors was within range 0.9–8.6%.

### 3.3. Computer simulations: examples

The tension simulations were conducted while attempting to reflect the conditions of the conducted experiments as accurately as possible (see point 2 in Direct Identification Methodology). The first simulation variant covered deformation in the solidification phase for the nominal test temperature of 1450°C, tool stroke rates of 1 and 20mm/s, and elongation of 2 mm. The basic aim of the simulation was to evaluate the suitability of the developed function

$\alpha$ [MPa <sup>-1</sup> ]	$n$	$A$ [s <sup>-1</sup> ]	$m$	$Q$ [J/mol]
5.4623641E – 02	0.2089816	1.65E+17	0.1855337	511111.2

**Table 1.** Identified parameters by the Direct Identification Methodology (DIM).

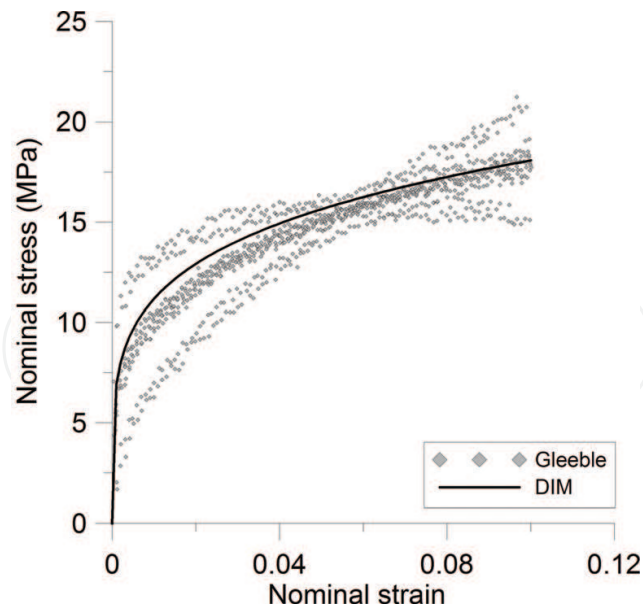


**Figure 21.** Comparison between measured (points) and calculated (line) stress-strain curve at the nominal temperatures of 1300°C and the nominal strain rate  $0.05 \text{ s}^{-1}$ .

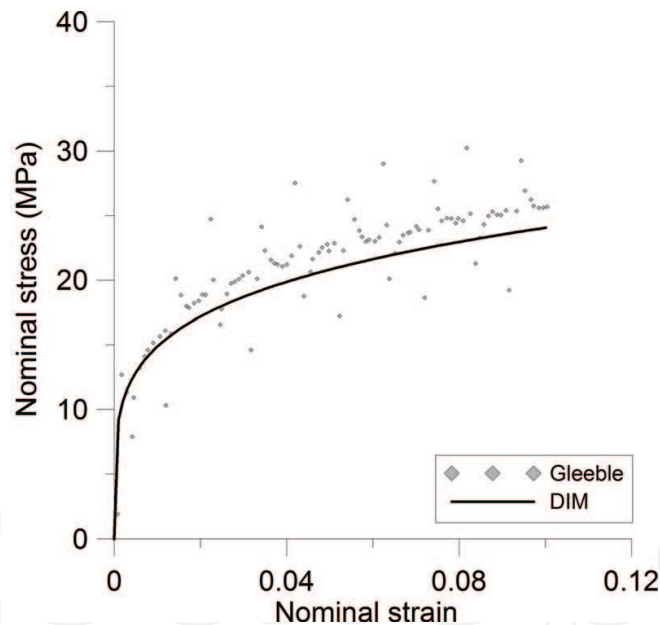


**Figure 22.** Comparison between measured (points) and calculated (line) stress-strain curve at the nominal temperatures of 1300°C and the nominal strain rate  $1 \text{ s}^{-1}$ .

describing changes in stress versus strain for the defined temperature range. **Figure 27** presents the initial temperature field for the nominal deformation test performed at a temperature of 1450°C using “hot” grips. The temperature difference between the sample surface and core was 33°C.

**Figure 28** presents the ultimate temperature distribution and the strain intensity after the tensioning process at a tool stroke rate of 1 mm/s and a grip stroke of 2 mm. Visualisations

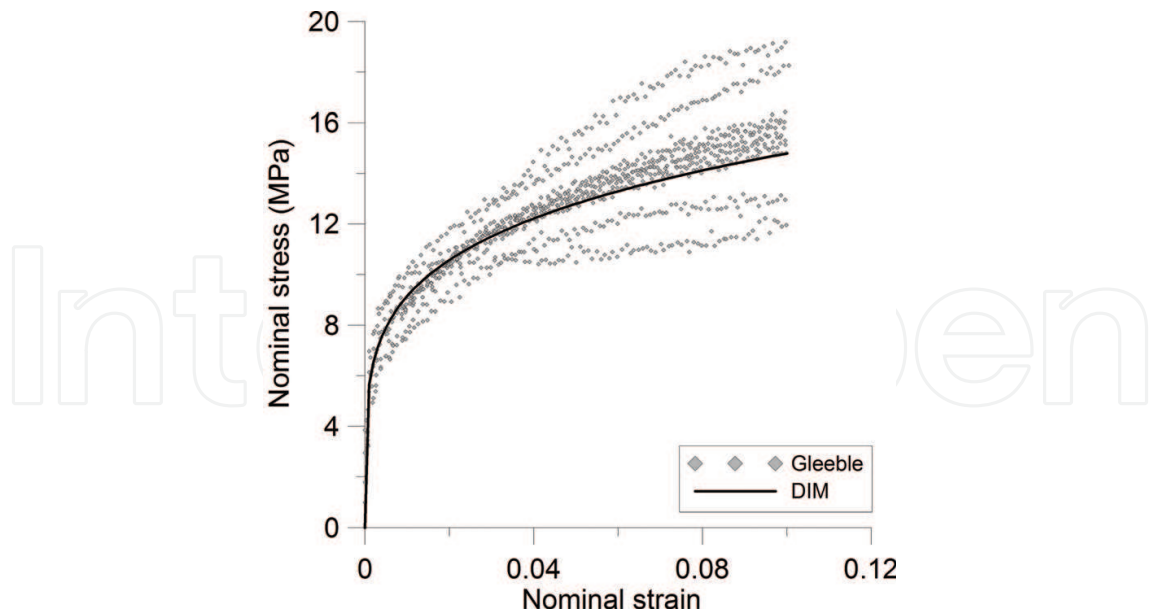


**Figure 23.** Comparison between measured (points) and calculated (line) stress–strain curve at the nominal temperatures of 1350°C and the nominal strain rate  $0.05 \text{ s}^{-1}$ .

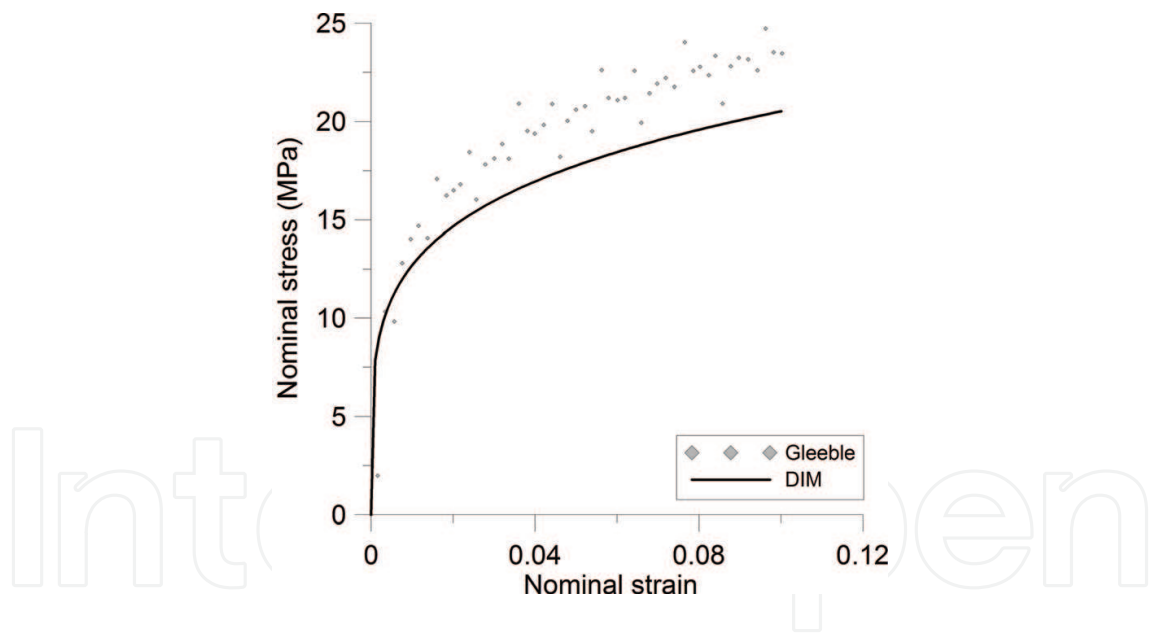


**Figure 24.** Comparison between measured (points) and calculated (line) stress–strain curve at the nominal temperatures of 1350°C and the nominal strain rate  $1 \text{ s}^{-1}$ .

were made along the sample maintaining the symmetry with respect to the Z axis. When analysing the temperature field after the resistance heating process (**Figure 27**), which at the same time is the initial condition for the mechanical solution, and the temperature field after the tensioning process (**Figure 28**), one may observe a slight reduction of the maximum temperature from 1483 to 1482°C. For the analysed temperature range even such small temperature changes within the deformation zone can cause rapid changes in the plastic and

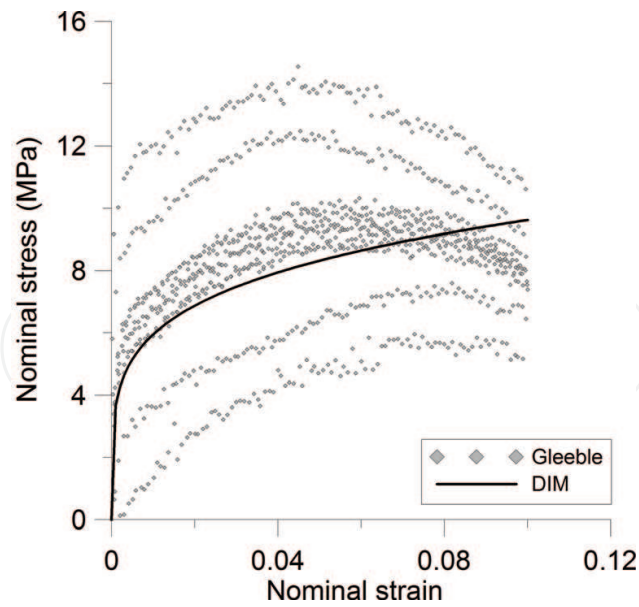


**Figure 25.** Comparison between measured (points) and calculated (line) stress-strain curve at the nominal temperatures of 1450°C and the nominal strain rate  $0.05 \text{ s}^{-1}$ .

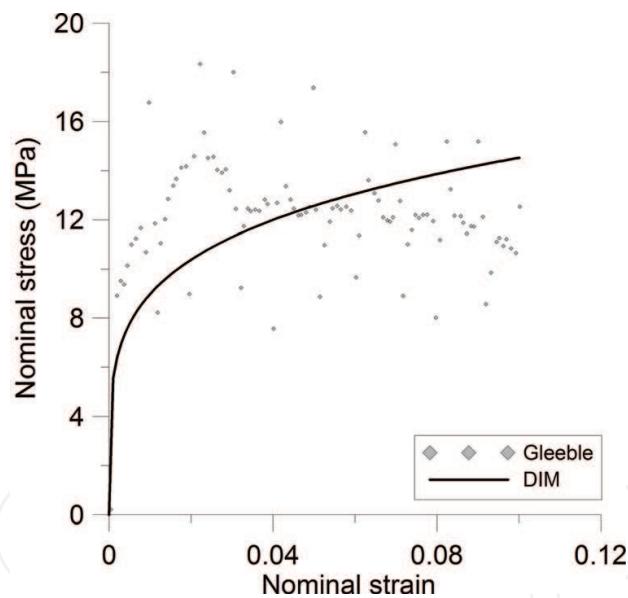


**Figure 26.** Comparison between measured (points) and calculated (line) stress-strain curve at the nominal temperatures of 1450°C and the nominal strain rate  $1 \text{ s}^{-1}$ .

mechanical properties. When analysing the obtained results one may observe a concentration of the maximum strain intensity values in the middle sample part.

In **Figures 29** and **30**, the comparison between measured and calculated loads at a nominal temperature of 1450°C and two stroke rates of 1 and 20mm/s is presented. The presented courses of loads changes feature a fairly large discrepancy between the measured and calculated loads. The obtained simulation results point that the application of the developed Direct Identification Methodology to determine parameters of the function describing changes leads

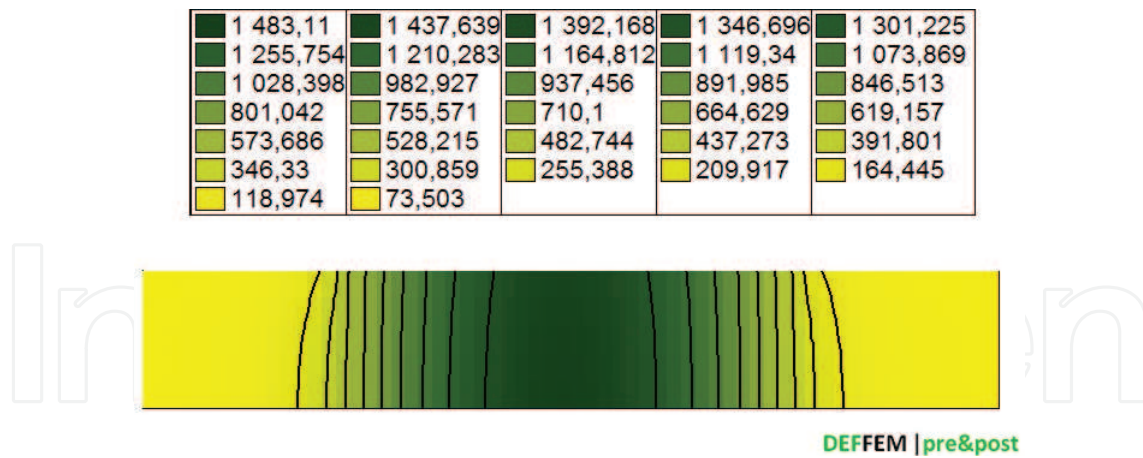


**Figure 27.** Temperature distribution on the sample section after heating and cooling to the nominal temperature of 1450°C (“hot” grips).

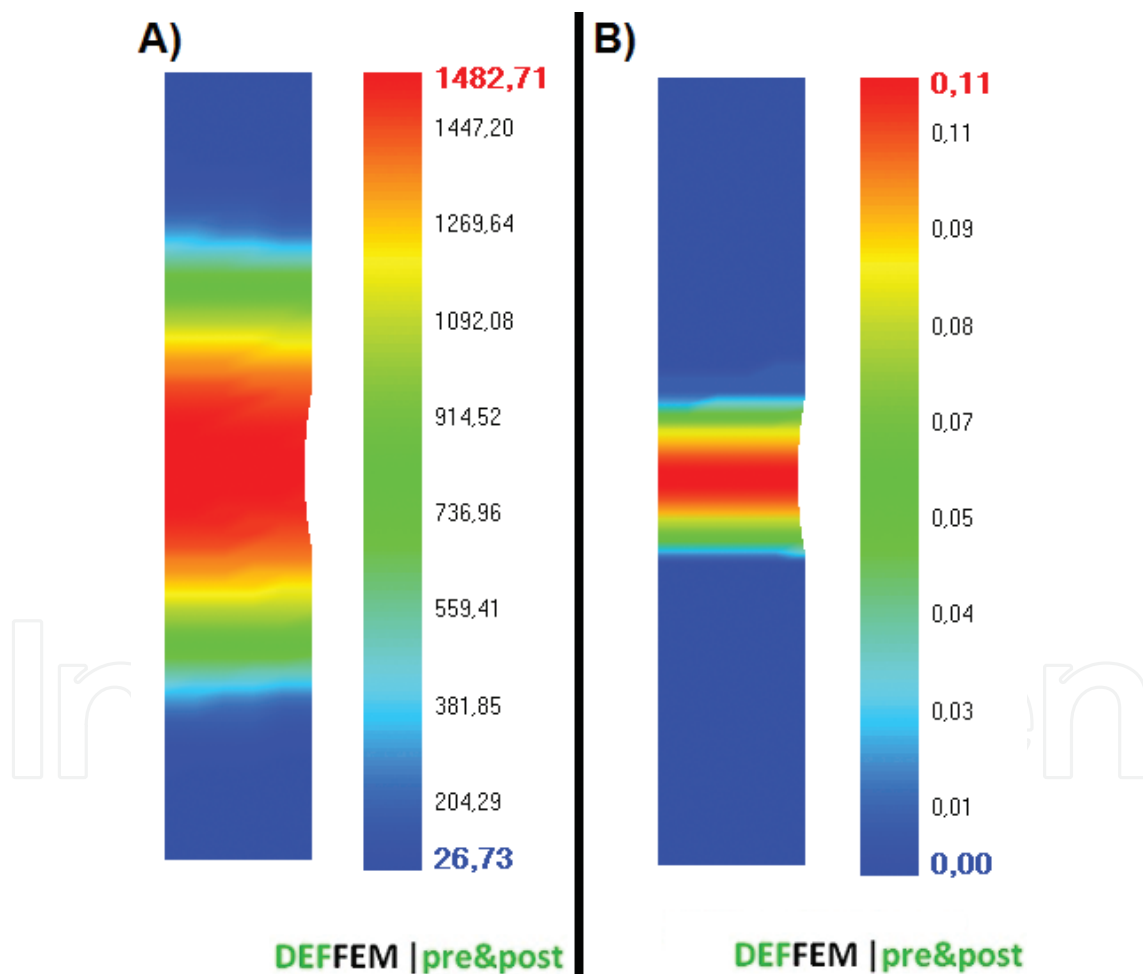


**Figure 28.** Distribution of (a) temperature (b) strain intensity on the cross-section of a sample deformed at the nominal temperature of 1450°C (“hot” grips, stroke rate 1mm/s, stroke 2mm).

to the final results. The average error value is at a level of 8.1% for the deformation variant at a temperature of 1450°C (stroke rate 1mm/s) and 19.1% for the test at a temperature of 1450°C (stroke rate 20mm/s). However, the obtained results indicate a certain non-uniformity of the

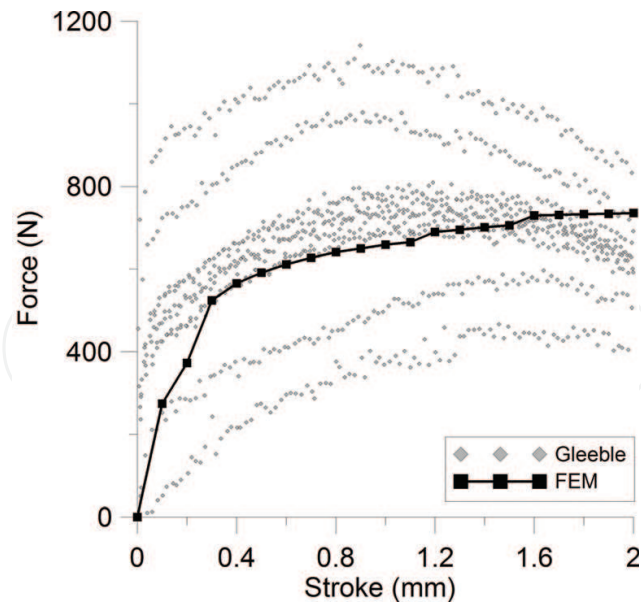


**Figure 29.** The comparison between measured and calculated loads at a nominal temperature of 1450°C and stroke rate of 1 mm/s.

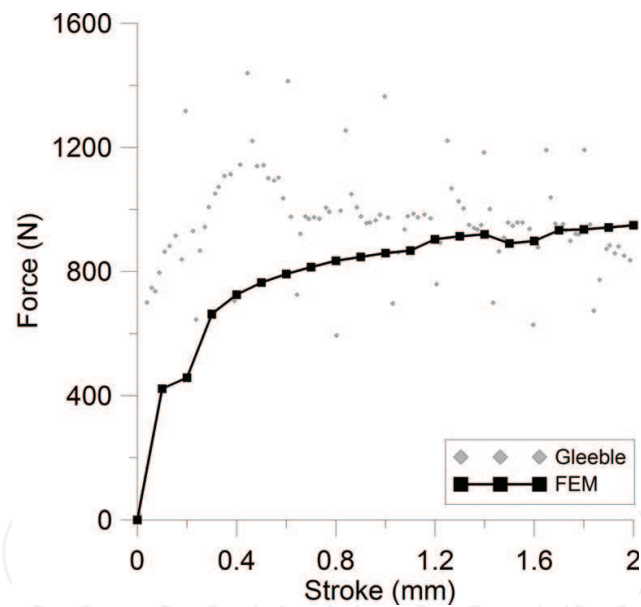


**Figure 30.** The comparison between measured and calculated loads at a nominal temperature of 1450°C and stroke rate of 20 mm/s.

deformation zone itself, as well as rapid changes in the plastic and mechanical properties along with a temperature change.

In the second variant, a pilot simulation of the integrated strip casting and rolling process was performed where the deformation was performed in two primary phases: crystallization

followed by the rough-rolling simulation. Conducting a multi-stage simulation required intensive implementation work and a partial reorganization of numerical codes in order to ensure transfer of strain and stress states, and the temperature field for the needs of the next stage simulation. The pilot physical and computer simulation included heating to a temperature of 1450°C at a rate of 20°C/s, and next to a temperature of 1485°C at a rate of 1°C/s in order to remelt the sample. The deformation process (compression) in the crystallisation phase was performed at a stroke rate of 0.25mm/s, a stroke of 1.5mm at a nominal temperature of 1460°C. Next, the sample was cooled at an average cooling rate of 50°C/s to the nominal rolling temperature of 1000°C. In the rolling process the sample was deformed (compressed) at a stroke rate of 1.25mm/s and a stroke of 4.0mm. The obtained results of the pilot numerical simulations were verified by comparison of the calculated and experimentally determined maximum force values at the individual stages, which are presented in **Table 2**.

At both stages the values of maximum forces calculated numerically were higher than the ones determined experimentally. The calculated relative error reached the maximum value of 13.77% for the stage of deformation at the crystallisation phase. Bear in mind that calculations within the DIM were performed for the adopted nominal test temperature equal to the surface temperature, and remember that the sample core temperature was higher by 33°C. Therefore, further research is necessary to determine the nominal temperature, e.g. adopting the core temperature as the nominal temperature, which effectively will allow the differences between the process force parameters to be reduced. The other essential fact influencing the obtained discrepancies in results of physical and computer simulations is lack of temperature field symmetry within the sample volume. From the perspective of the essence of the axially symmetrical numerical model and the computing accuracy, the temperature field in each section plane in ideal conditions should be the same or very similar. **Figure 31** presents a picture from a NANOTOM N190 tomograph showing the formed porous zone. The visible porous zone formed starting from the sample core, propagating towards the sample surface (place of installation of the control thermocouple TC4, see **Figure 1**). It is the place where the sample surrounded by a quartz shield has a 2–3mm gap enabling thermocouples to be installed. The other areas are thermally insulated, and the said gap is the main source of disturbances in the heat exchange between the sample and its environment (simulator inside). Therefore, one may conclude that the elimination of the quartz shield combined with the precise control of the process (manual control) will allow lack of the temperature field symmetry to be eliminated. As a result, the obtained results of numerical simulations should feature a higher accuracy.

	Solidification stage [N]	Rolling stage [N]
Physical simulation	617	7144
Computer simulation	702	7737
Relative error	13.77%	8.30%

**Table 2.** Comparison of the maximum forces determined experimentally and numerically at the individual stages.

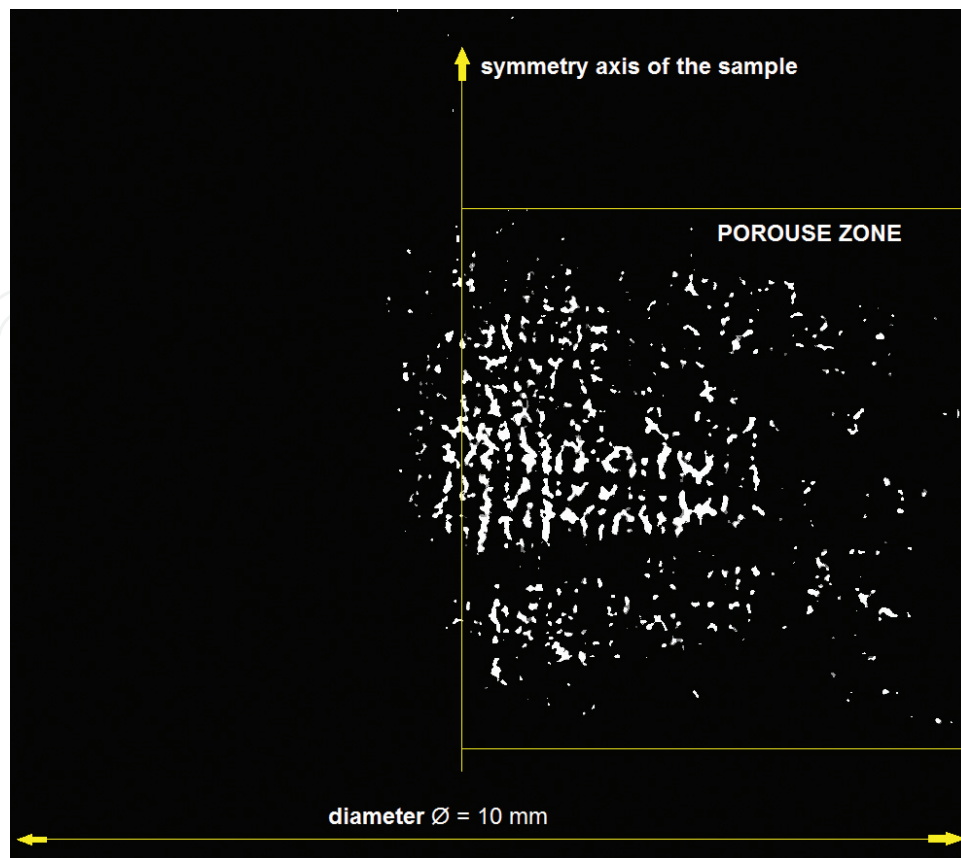


Figure 31. A longitudinal section with a visible formed porous zone (“hot” grips, cylindrical sample heating zone centre).

## 4. Conclusions

The primary aim presented in this chapter is to show experimental and modelling problems related to research aiming at obtaining data necessary to develop a physical model of steel deformation in the semi-solid state. The computer aid to the experiment, using the process computer simulation, is an inherent part of the presented methodology. It is difficult to imagine experimental research of steel deformed during the final solidification phase without this simulation. This issue is strictly related to the signalled problems related to the application of the soft-reduction process. The formulated resistance heating model in the simulator system and the computer-aided methodology of direct determination of mechanical properties of the steel tested allowed the preliminary concept of multi-stage modelling (integrated casting and rolling process) to be developed with the DEFFEM package. The obtained results in the form of force parameters feature a correct compatibility, albeit constraints resulting from the application of axially symmetrical models indicate new trends in the development of models and methods. In order to fully describe the behaviour of the semi-solid steel during its deformation in the integrated casting and rolling process the constructed mathematical model must be fully three-dimensional. The necessity of application of spacial models arises from the fact of existence of zones in high temperatures: the solid and semi-solid zone, many's the time having a complex geometrical shape. Such models should be applied to the issue concerned regardless

of the fact that traditional strip rolling processes in the hot metal forming conditions can be modelled in the flat strain condition.

## Acknowledgements

The research has been supported by the Polish National Science Centre (2012–2017), Decision number: DEC-2011/03/D/ST8/04041

## Author details

Marcin Hojny

Address all correspondence to: [mhojny@metal.agh.edu.pl](mailto:mhojny@metal.agh.edu.pl)

AGH University of Science and Technology, Kraków, Poland

## References

- [1] Project report. (AGH Krakow-IMZ Gliwice); Number: B0–1124, 2010 (not published)
- [2] Bald W, et al. Innovative technologies for strip production. *Steel Times International*. 2000;**24**:16–19
- [3] Cook R, Grocock PG, Thomas PM et al. Development of the twin-roll casting process. *Journal of Materials Processing Technology*. 1995;**55**:76–84
- [4] Fan P, Zhou S, Liang X et al. Thin strip casting of high speed steels. *Journal of Materials Processing Technology*. 1997;**63**:792–796
- [5] Park CM, Kim WS, Park GJ. Thermal analysis of the roll in the strip casting process. *Mechanics Research Communications*. 2003;**30**:297–310
- [6] Seo PK, Park KJ, Kang CG. Semi-solid die casting process with three steps die system. *Journal of Materials Processing Technology*. 2004;**154**:442–449
- [7] Watari H, Davey K, Rasgado MT et al. Semi-solid manufacturing process of magnesium alloys by twin-roll casting. *Journal of Materials Processing Technology*. 2004;**156**:1662–1667
- [8] Głowacki M, Hojny M, Kuziak R. Komputerowo wspomagane badania właściwości mechanicznych stali w stanie półciekłym. Kraków: Wyd. AGH; 2012
- [9] Hojny M. Projektowanie dedykowanych systemów symulacji odkształcania stali w stanie półciekłym. Krakow, Poland: Wzorek; 2014

- [10] Hojny M. Modeling of steel deformation in the semi-solid state. In: *Advanced Structured Materials*. Vol. 78. Springer, Switzerland; 2017
- [11] Hojny M, Siwek A. Computer and physical modeling of resistance heating in the Gleeble 3800 simulator. *Proc. KomPlasTech conference, 17–20 stycznia, 2016, Wisła, Poland*, pp. 66–67
- [12] Hojny M, Glowacki M. Computer modelling of deformation of steel samples with mushy zone. *Steel Research International*. 2008;**79**:868–874
- [13] Hojny M, Glowacki M. The physical and computer modelling of plastic deformation of low carbon steel in semi-solid state. *Journal of Engineering Materials and Technology*. 2009;**131**:041003-1-041003-7
- [14] Hojny M, Glowacki M. Modeling of strain-stress relationship for carbon steel deformed at temperature exceeding hot rolling range. *Journal of Engineering Materials and Technology*. 2011;**133**:021008-1-021008-7
- [15] Hojny M, Głowacki M, Malinowski Z. Computer aided methodology of strain-stress curve construction for steels deformed at extra high temperature. *High Temperature Materials and Processes*. 2009;**28**(4):245-252. ISSN 0334–6455
- [16] Szyndler D. Problem odwrotny w zastosowaniu do identyfikacji parametrów procesu plastycznej przeróbki metali. PhD. thesis. Krakow; 2001